Biosensors and Bioelectronics: X 25 (2025) 100624

Contents lists available at ScienceDirect

Biosensors and Bioelectronics: X

journal homepage: www.journals.elsevier.com/biosensors-and-bioelectronics-x

Synthesis of nickel dopped chitosan nanoparticles as a novel platform for electrochemical insulin detection

Frederika Chovancová [a], Marjan Motiei [b], Ivana Šišoláková [a,*], Michal Urbánek [b], Jana Shepa [a], Haojie Fei [b], Petr Sáha [b], Renáta Oriňaková [a,b]

[a] Department of Physical Chemistry, Faculty of Science, Pavol Jozef Šafárik University, Moyzesova 11, 040 01, Košice, Slovak Republic
[b] Centre of Polymer Systems, Tomáš Baťa University in Zlín, Třída Tomáše Bati 5678, 7601, Zlín, Czech Republic

ARTICLE INFO

Keywords:
Nickel
Chitosan nanoparticles
Insulin
Sensor
Electrochemistry

ABSTRACT

Nickel modified chitosan nanoparticles are promising catalysts for the determination of bioanalytes such as insulin, glucose, antibiotics, and ascorbic acid. In this study, we synthesized nickel-loaded chitosan nanoparticles to evaluate their potential as surface modifiers for electrochemical sensors for insulin detection. The nanoparticles were prepared using the ionic gelation of chitosan with tripolyphosphate anions, followed by adsorption of nickel ions via ion-exchange resins and surface chelation. The physicochemical properties of the nanoparticles were characterized by scanning electron microscopy with EDX analysis, transmission electron microscopy, Fourier-transform infrared spectroscopy, and dynamic light scattering. The catalytic activity of nickel modified chitosan nanoparticles towards insulin oxidation was investigated through cyclic voltammetry. The resulting screen-printed carbon electrode modified with nickel-chitosan nanoparticles exhibited exceptional analytical performance, including high sensitivity (0.09 mA μM), a low detection limit (0.02 μM), and a wide dynamic range (300 nM–5 μM). Additionally, the modified screen-printed electrode demonstrated excellent selectivity, enabling accurate insulin determination in the presence of interferences and in real blood serum samples. These findings highlight the potential of nickel-modified chitosan nanoparticles as a surface modification strategy to enhance the performance of electrochemical sensors insulin detection and pave the way for their application in various bioanalytes determination platforms.

1. Introduction

Chitosan, derived from chitin found in crustaceans and insects (Yanat and Schroën, 2021; Vroman and Tighzert, 2009) has garnered extensive interest due to its diverse chemical, biological, and physical properties, including biodegradability, hydrophobicity, low toxicity, bioavailability, antimicrobial activity. It has the potential to be extended in various biomedical applications, such as tissue engineering, drug delivery and biosensors (Islam et al., 2017; Othman et al., 2021). Its structure's amino and hydroxyl groups give it several biological qualities, including antibacterial and antioxidant effects (Vicente et al., 2025). Chitosan has a special polycationic property that makes it soluble in acidic aqueous environments, because its amino groups protonated in acidic solution. On the other hand, chitosan becomes insoluble in an alkaline environment because the amino groups lose their positive charges (Seyam et al., 2024). Chitosan's stability and use are limited by the solubility in media various pH as was mentioned above. Cross-linked chitosan nanoparticles could be created by altering its molecular structure, which would get around these problems (Vicente et al., 2025). To create chitosan nanoparticles, several chemical and physical processes have been developed, including spray drying, top-down approaches, ionic gelation, crosslinking, emulsification, and precipitation-based methods (El-Naggar et al., 2024).

Chitosan nanoparticles (CSNPs) are predominantly synthesized through the ionic (ionotropic) gelation method using polyanion sodium tripolyphosphate (TPP) (Motiei et al., 2017; Simos et al., 2021; Ribeiro et al., 2018) and they have exhibited tremendous potential in diverse medical applications, including drug delivery, pharmacy, and electrochemical sensors (Yanat and Schroën, 2021; Khoerunnisa et al., 2021). Despite these advantageous properties, the low conductivity of chitosan poses a limitation for its application in electrochemical sensors. To address this challenge, researchers doped chitosan with various metal species to improve its conductivity (Simos et al., 2021). Because of their annulus chelating structure and natural enzyme characteristics, chitosan

* Corresponding author.
E-mail address: ivana.sisolakova@upjs.sk (I. Šišoláková).

https://doi.org/10.1016/j.biosx.2025.100624
Received 3 December 2024; Received in revised form 4 March 2025; Accepted 18 April 2025
Available online 3 May 2025

metal complexes generally show favorable catalytic activity for a wide range of chemical reactions. For the electrooxidation of formaldehyde, a catalyst based on nickel ions distributed onto a carbon paste electrode modified with chitosan was created (Mao et al., 2017). Based on previous research, Ni nanoparticles (NiNPs) represent an ideal candidate for advanced electrochemical insulin sensors (Šišoláková et al., 2023; Shepa et al., 2021; Hovancová et al., 2017). The catalytic activity of NiNPs lays in the formation of NiOOH species under alkaline pH conditions (Šišoláková et al., 2021; Yu et al., 2016).

Insulin, a vital peptide hormone, is naturally produced by the islets of Langerhans located in the pancreas (Shepa et al., 2021; Hovancová et al., 2017). This hormone plays a crucial role in various metabolic processes (Cruz-Pineda et al., 2022) and the regulation of glucose levels (Shepa et al., 2021), which causes hyper- or hypoglycaemia.

Consequently, the development of electrochemical sensors for efficient and cost-effective insulin detection is imperative for enhancing diabetes diagnosis. Due to the relatively low insulin concentration in the blood (0.86 μM) (Šišoláková et al., 2020, 2021i, 2021šoláková et al., 2020) only a few analytical methods are used in clinical diagnostic practices (Hovancová et al., 2017; Hovancova et al., 2018). The predominant issues associated with current methods like high performance liquid chromatography and capillary electrophoresis include their financial demands, prerequisite pre-treatment steps, and the need for skilled personnel to operate the specialized equipment (Hovancová et al., 2017; Parasuraman et al., 2015; Przybylska et al., 2021). Electrochemical sensors designed for direct insulin oxidation have the potential to overcome the aforementioned challenges (Šišoláková et al., 2021, 2023i, 2023šoláková et al., 2021). In general, electrochemical sensors offer fast response, easy data analysis, and economic viability (Ibáñez-Redín et al., 2018; Dong et al., 2020). Screen-printed carbon electrodes (SPCE) are increasingly popular among the electrochemical sensors due to their compact design. These electrodes offer a cost-effective solution and only require a minimal sample volume of 50 μL for precise measurements. Their affordability and efficiency position them as an excellent option for biomedical applications (Šišoláková et al., 2020; Musa et al., 2021; Ivanov et al., 2021).

Here, we aim to synthesize Ni-modified CSNPs for potential application in SPCE based electrochemical sensor designed for insulin detection, using the TPP as a crosslinking agent for preparation chitosan nanoparticles. The present work focused on enhancement of the electroanalytical properties of electrochemical sensors modified by chitosan.

2. Methods

2.1. Chemicals and reagents

Insulin Human Recombinant, and Phosphate Buffered Saline (d 8662, sterile filtered) were purchased from Biowest (Kansas City, USA). Potassium ferricyanide trihydrate (99.95 %), potassium ferrocyanide trihydrate, (99.95 %), ascorbic acid (99 %), uric acid (99 %), chitosan (low molecular weight), sodium tripolyphosphate (85 %), potassium chloride (99 %), Polysorbate 80, ethanol (98 %), sodium hydroxide (99 %), hydrochlorid acid (37 %), and human blood serum were purchased from Sigma Aldrich (Missouri, USA). Nickel chloride hexahydrate (99 %) was purchased from CentralChem (Bratislava, Slovakia).

2.2. Instrumentations

All electrochemical measurements were performed using a Metrohm AUTOLAB PG- STAT302N potentiostat (Utrecht, Netherlands) controlled using Nova 1.10 software, combined with a connector for the SPCE. Metrohm SPCEs type DRP-11L (Utrecht, Netherlands) have been used for all electrochemical experiments. Used SPCEs consist of three electrodes (working electrode = carbon electrode, auxiliary electrode = carbon electrode, pseudoreference electrode = silver/silver chloride electrode) printed on the ceramic substrate (L = 33 mm x W = 10 mm x H = 0.5 mm). Silver/silver chloride reference electrode was used as a pseudoelectrode without any modification prior to the electrochemical measurements. All electrochemical experiments were conducted at the laboratory temperature and atmospheric pressure. The structure and surface morphology of the electrodes were characterized using Scanning Electron Microscope (SEM) Nova NanoSEM 450 (The Netherlands, FEI Company). The SEM energy dispersive X-ray (EDX) analysis was performed with EDX spectrometer Octane Plus (EDAX, AMATEK, Inc). SEM and EDX analyses of CSNPs and Ni-CSNPs were performed on a piece of aluminum foil by drying the samples prior to analysis. TEM analysis was realized via Transmission Electron Microscope (JEOL JEM 2100, Japan) operated at an acceleration voltage window to 200 kV with a brightness LaB6 source. The size of nanoparticles was calculated from TEM images using ImageJ software (version 4.8). Samples for TEM analysis were dropped on the surface of copper grid with molded membrane. Dynamic light scattering analysis (ZETA NANO ZS ZEN3601 Malvern, UK) was used to evaluate the particle size, Zeta potential and electrical conductivity of the prepared nanoparticles. The pH was controlled using pH meter (Lab 845 pH Meter; SI Analytics). FT-IR spectra were collected with a Nicolet iS5 spectrometer at 64 scans and a resolution of 4 cm^{-1} over a wavenumber range of 4000–400 cm^{-1} when liquid samples (CSNPs, Ni-CSNPs, and TPP) were dried at 30 °C for 24 h and atmospheric pressure in dryer. Dried, solid samples were used for FT-IR analysis.

2.2.1. CSNPs and Ni-CSNPs preparation

CSNPs were synthesized following the procedure outlined by Motiei et al. (Dong et al., 2020) via the ion-gelation method. Initially, 50 mg of powdered low molecular weight chitosan (50–190 kDa) was dissolved in 50 ml 1 % (w/v) aqueous acetic acid solution and subjected to stirring at room temperature for 24 h. The pH of the resultant chitosan solution was adjusted to 4.8 using 1M NaOH. Subsequently, Polysorbate 80 was added to the chitosan solution to achieve a concentration of 0.5 %w/v. The mixture was stirred at 650 rpm within a temperature range of 45–50 °C for 2.5 h to attain a homogenous colloidal dispersion. Notably, the size of CSNPs can be affected by many factors such as stirring time, speed, temperature, chitosan concentration, pH of chitosan solution, and primarily, the chitosan to TPP ratio (Nayak). Therefore, concentration of 10 mg/mL of TPP in deionized water with pH value of 8 was prepared, and then four different volumes of TPP (100 μL, 120 μL, 140 μL, and 160 μL) were added into the 3 mL of prepared chitosan solution under stirring at 650 rpm using magnetic stirrer for 30 min at room temperature. Subsequently, their polydispersity index (PDI) and hydrodynamic diameter (HD) of the nanoparticles were determined. All DLS measurements were performed at the same size cuvette, and the same volume 3 mL of CSNPs was used for it. The resulting nanoparticles were subjected to centrifugation at 10.000 rpm for 15 min to facilitate separation. To produce Ni-CSNPs, a solution containing 200 μL of 0.06 M $NiCl_2.6H_2O$ was gradually introduced into the prepared colloid of chitosan nanoparticles. The mixture was stirred at 450 rpm for 30 min at room temperature, then the nanoparticles were subjected to centrifugation at 10.000 rpm for 15 min to isolate the final product.

2.2.2. Development of CSNPs and Ni-CSNPs SPCEs

Bare SPCE was washed with ethanol for purification. 10 μL of prepared CSNPs or Ni-CSNPs were dropwise added on the surface of working carbon electrode and dried at laboratory temperature. After modification, SPCEs were activated in 0.1 M NaOH solution via CV in potential range 0.1 V–0.7 V at a scan rate of 100 mV/s for 10 cycles. Activation under alkaline conditions is essential, because $Ni(OH)_2$ species are generated at alkaline pH levels because it is necessary to change nickel complexed with chitosan to the $Ni(OH)_2$.

2.2.2.1. Insulin solution preparation. Calculated mass of powdered

insulin was dissolved in phosphate-buffered saline (PBS) with 0.1 M NaOH to get various insulin concentrations (0.3 μM–5 μM). In case of interference samples testing, the interference samples were prepared in phosphate-buffered saline (PBS) without insulin present in the solution. To study the electrochemical determination of insulin in real samples powdered insulin was dissolved in human blood serum and 0.1 M NaOH. All samples were freshly prepared before each measurement.

3. Results and discussion

3.1. Characterization of CSNPs and Ni-CSNPs

3.1.1. Polydispersity index and hydrodynamic diameter of CSNPs

DLS was used to assess PDI and the average HD of the synthesized nanoparticles. The determination of the average HD of CSNPs was performed in different volumes of TPP solution (100 μL, 120 μL, 140 μL, and 160 μL) at a concentration of 10 mg/mL and pH 8. Table 1 summarizes the PDI and HD of the prepared CSNPs. Each measurement was performed five times, and the average values were tabulated. TPP was used for cross-linking by ionic gelation. In this process, polyanions ($P_3O_5^{-10}$) interact with positively charged amino groups of chitosan via electrostatic forces and create ionic cross-linked networks (Vicente et al., 2025). The results show that the addition of TPP in volumes of 160 μL and 140 μL chitosan solution at alkaline pH yielded increased PDI values of 0.82 and 0.60, respectively. These values indicate an aggregation process within the prepared CSNPs, which is characterized by a PDI value exceeding 0.5 (Šišoláková et al., 2020). When the TPP volume decreased to 120 μL and 100 μL, the PDI value also decreased, reaching a lower value of 0.44 and 0.47, respectively.

The HD of the resultant nanoparticles reached its minimum at 84.7 nm in the sample containing 160 μL of TPP. However, considering the high PDI value associated with this sample, the use of 160 μL of TPP is not suitable for future CSNPs preparation, as it would compromise optimized properties. For an optimal balance between HD and PDI, a sample with the addition of 100 μL of TPP is the more suitable. Here, PDI and HD were determined as 0.47 ± 0.041 and 195.0 ± 42.47 nm, respectively. 100 μL of TPP was selected as the optimal choice due to the PDI is less than 0.5 and the particles are smaller compared to 120 μL. Smaller particles potentially exhibit more particles at the surface of WE (diameter 4 mm) and could provide more active surface sites for the Ni-modified CSNPs. The hypothesis is, therefore, that this will enhance the current response and improve analytical parameters. The PDI parameter is indicative of the homogeneity of the prepared samples. According to the literature, a PDI value of less than 0.5 is ideal. A PDI value greater than 0.5 suggests that the particles are aggregating (Algharib et al., 2022). From the electrochemical sensors point of view, the homogeneity of prepared samples is the key factor in sensor preparation at least from electrode material uniformity and sensor reproducibility. Consequently, CSNPs formulated with an addition of 100 μL of TPP were selected for all subsequent experiments.

3.1.2. Zeta potential and electrical conductivity

Zeta potential and electrical conductivity were employed to determine the stability of the prepared colloidal systems for both CSNPs and Ni-CSNPs samples. To ensure reproducibility, all measurements were carried out in triplicate. Based on the previous results, CSNPs synthesized with the addition of 100 μL of TPP were selected for further analysis. The colloidal CSNPs system showed an average value of Zeta potential of 14.4 mV, and electrical conductivity of 6.69 mS/cm. Similarly, for Ni-CSNPs, the Zeta potential of 12.47 mV was determined, while the conductivity stood at 6.72 mS/cm. The small alteration in Zeta potential with Ni is due to charge screening, surface complexation between Ni^{2+} and the functional groups of chitosan, and the minimal quantity of $NiCl_2$ added. The observed Zeta potential values indicate the stability of CSNPs and NiNPs, as they fall within the range of 10 mV–20 mV, which is known to ensure the stability of colloidal systems (Bhattacharjee, 2016). Based on the literature, the solutions of chitosan with the same concentration display at least 3-times lower conductivity (approx. 2 mS/cm). So, the CSNPs creation improve the conductivity of prepared material (Le et al., 2018). The relatively close values of conductivity in the prepared colloidal systems could be attributed to the addition of only 200 μL of 0.06 M $NiCl_2$ into a 3 ml of colloidal system composed of CSNPs. Furthermore, the introduction of Ni into the CSNPs did not lead to significant changes in Zeta potential. According to existing literature, metallic nanoparticles such as Ni, Cu, and Bi, as well as metal oxide nanoparticles NiO, typically exhibit negative Zeta potential values. It's worth noting that the zeta potential of metal nanoparticles can also be affected by solution concentration and pH (Kuyukina et al., 2022). It is necessary to mention that the Ni is not in the form of metal particles but creates the complex with Ni^{2+}ions. In our investigation, nickel was introduced as a $NiCl_2$ solution containing Ni^{2+} ions. Nickel is not presented as metallic nickel (Ni^0) or in solid form. Rather, Ni^{2+} ions creating complex with chitosan instead of existing as separate metallic entities. In general, the binding of transition metal ions by chitosan is realized by coordination with the amino (-NH_2) and/or hydroxy (-OH) groups. The chitosan chains serve as coordination sites. The Mentioned groups are grabbed by one nickel ion and form the chitosan-nickel complex. The mechanism of the formation is the following:

$$(CH) - NH_2 + H_3O^+ \rightarrow (CH) - NH_3^+ + H_2O \quad (1)$$

$$Ni(OH)_2 \leftrightarrow Ni^{2+} + 2OH^- \quad (2)$$

$$Ni^{2+} + (CH) - NH_3^+ \leftrightarrow (CH) - NH_2Ni^{2+} + H^+ \quad (3)$$

Based on the literature, the immersion of prepared chitosan materials into the 0.1 M NaOH causes irreversible changes in chemical and physical properties of the membrane. So, in our case it could be expected that the prepared material becomes insoluble and Ni^{2+} turns into insoluble nickel hydroxide particles(Ciszewski and Stepniak, 2013).

$$(CH) - NH_2Ni^{2+} + 2OH^- \rightarrow (CH) - NH_2 + Ni(OH)_2 \quad (4)$$

3.1.3. Fourier-transform infrared spectroscopy analysis

FT-IR is a valuable technique for confirming chemical composition, identifying functional groups, and elucidating potential intermolecular interactions. FT-IR spectra of NPs and neat samples including CS, TPP and $NiCl_2.6\,H_2O$ are shown in Fig. 1. The IR spectra of pure CS exhibited distinct characteristic peaks, including those at 902 cm^{-1} (associated with the pyranose ring), 3373 cm^{-1} (indicating OH and NH_2 stretching), 2881 cm^{-1} (reflecting –CH stretching), 1656 cm^{-1} (corresponding to amide I), 1594 cm^{-1} (representing amide II), 1373 cm^{-1} (linked to CH_3 symmetrical deformation mode), and 1068 cm^{-1} (reflecting asymmetric C–O–C stretching)(Motiei et al., 2017). The peak at 1068 cm^{-1} based on some literature sources pertain to P=O vibrational stretch which was found in previous study for the CSNPs (Motiei et al., 2020).

In the spectrum of $NiCl_2.6H_2O$ the broad absorption bands in the range of 1600-1400 cm^{-1} can be attributed to bending vibrations of O-H bonds from water and vibrations associated with chloride ions. Distinct absorption peaks with notable maxima at 3056 and 3207 cm^{-1} were observed in the high-frequency region 3500-3200 cm^{-1}, representing the symmetric and asymmetric valence vibrations of water. The peak at about 3592 cm^{-1} typically indicates the stretching vibration of the Ni-

Table 1
Effect of added to TPP on particles size and PDI in alkaline conditions.

Volume of TPP (μL)	Hydrodynamic diameter (nm)	Polydispersity index
160	84.7 ± 31.13	0.82 ± 0.13
140	209.7 ± 132.22	0.60 ± 0.15
120	246.8 ± 55.42	0.44 ± 0.03
100	195.0 ± 42.47	0.47 ± 0.04

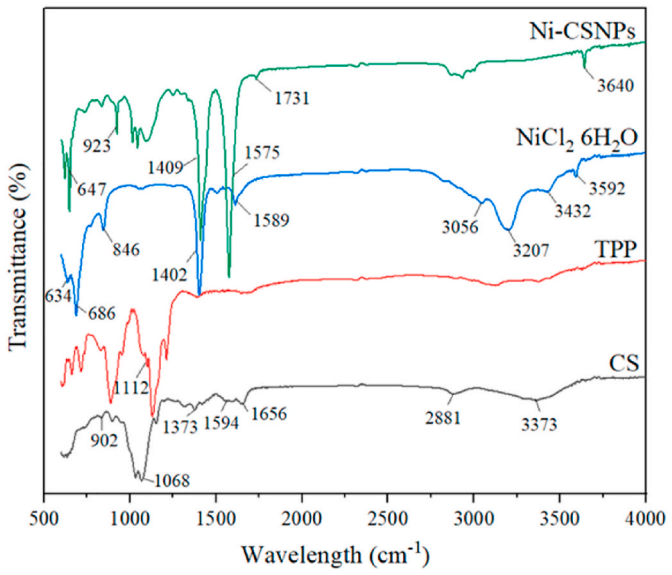

Fig. 1. FT-IR spectra of NPs and neat samples including CS, TPP and $NiCl_2.6\ H_2O$.

oxygen (Ni-O) bond, which results from interactions between the Ni cation (Ni^{2+}) and the chloride anions (Cl^-) in the compound. The presence of weakly bound water in metal hydrates is expressed by the spectrum at 3432 cm^{-1}. Bands in the range of 1300-1000 cm^{-1} correspond to stretching vibrations of Ni-oxygen (Ni-O) bonds, Ni-chlorine (Ni-Cl) bonds, and other Ni-ligand interactions (Netskina et al., 2020).

Analysis of the nanoparticle Ni-CSNPs spectra revealed sharp high-intensity bands, including peaks at 1575 cm^{-1} (Amide II band), 1409 cm^{-1} (symmetric stretching of COO−), and 647 cm^{-1} (weak N–H stretching vibrations). The significant shift of the peaks at 3592, 1589, and 1402 cm^{-1} after Ni (II) adsorption can be attributed to the Ni adsorption sites on the NPs, specifically interacting with the nitrogen atom of the amine group. Evidently, other prominent peaks at 923 cm^{-1}, 1041 cm^{-1}, and 1043 cm^{-1} on the NPs indicate the phosphate group of TPP intervention. This suggests that the adsorption process involves electrostatic interactions and complex formation between functional groups, especially the phosphate group of TPP, the amine group of CS on the surface of NPs, and the Ni (II) ions (Naskar et al., 2016).

3.1.4. Size recognition study of CSNPs and Ni-CSNPs

SEM was used to study surface morphology, and TEM was used to investigate the size of synthetized particles CSNPs and Ni-CSNPs. EDX analysis was utilized to identify the elemental composition of both CSNPs and Ni-CSNPs. The nanoparticle sizes were determined using ImageJ software and were then compared with values obtained from DLS. Fig. 2 illustrates the SEM (Fig. 2A), and TEM (Fig. 2B) images of CSNPs at scale 20 μm and 0.2 μm, accompanied by EDX analyses (Fig. 2C). The SEM and TEM images demonstrated the presence of spherical CSNPs structures with an average calculated size of approximately 134.1 nm. A histogram showing the size of CSNPs based on TEM images is shown in Fig. 2D. Notably, the size of CSNPs derived from TEM (Fig. 2B) appeared to be significantly smaller than that obtained from DLS measurements. DLS measures the hydrodynamic diameter, which includes the hydration shell around the nanoparticles. Chitosan is a hydrophilic polymer that absorbs water and forms a hydrated shell in solution, making the particles appear larger in DLS analysis. When dried, the water content is removed, leading to a reduction in apparent size. The key reason for the smaller sizes of chitosan nanoparticles in the dried state is the absence of the hydration layer, combined with polymer shrinkage, solvent evaporation, and increased intermolecular interactions. The DLS-measured size is always larger due to the influence of water, while the dried particles reflect their true core dimension (Bhattacharjee, 2016).

On the other hand, the analysis after drying is necessary for it to be further used as an electrode material. In the SEM image (Fig. 2A), the

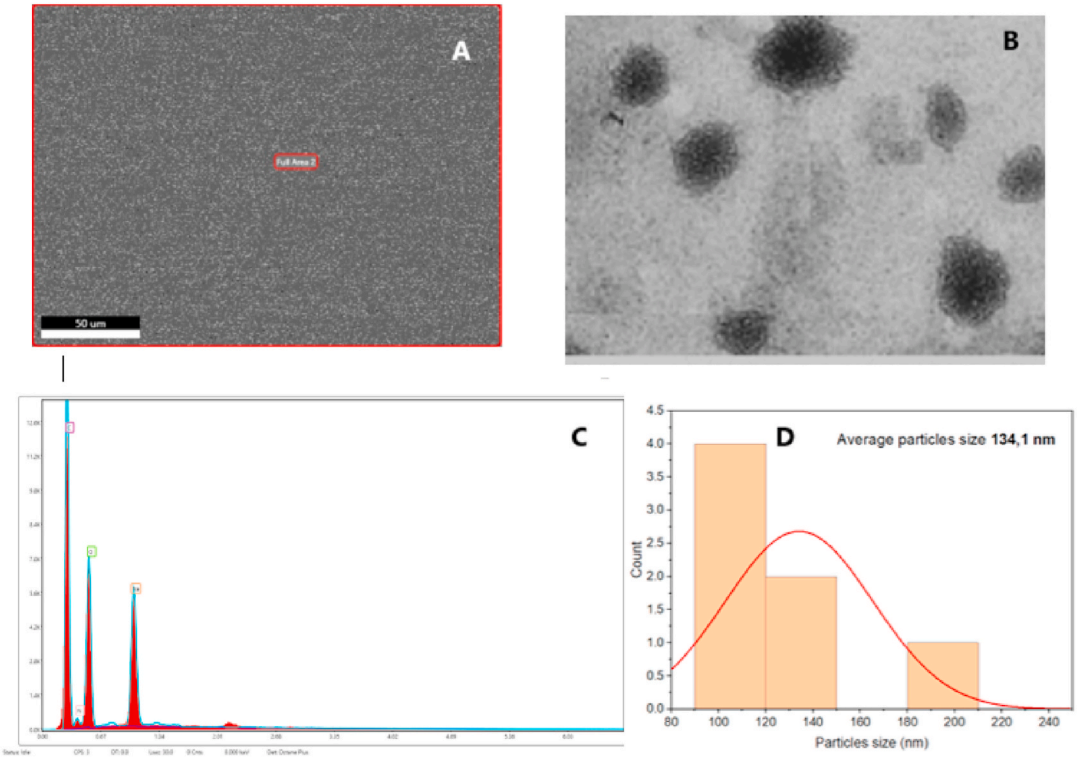

Fig. 2. SEM image of CSNPs at a scale of 50 μm (A). TEM image of CSNPs at scale of 0.2 μm (B), EDX spectrum of CSNPs (C) and histogram (D) of CSNPs size according to TEM image.

area that was subjected to EDX analysis is marked in red. The EDX elemental analysis revealed the presence of 52.3 wt% carbon, 27.6 wt% oxygen, 18.0 wt% sodium, and 2.2 wt% of nitrogen. The presence of sodium can be attributed to the use of sodium salt of TPP as a cross linker and 1 M NaOH for pH adjustment during the CSNPs preparation.

Fig. 3 shows the SEM (Fig. 3A) and TEM (Fig. 3B) images of Ni-CSNPs at scales of 20 μm, and 0.5 μm, respectively, along with corresponding EDX analysis (Fig. 3C). A spherical structure of Ni-CSNPs was observed like that observed in the CSNP sample. The average size of Ni-CSNPs, calculated from the TEM image (Fig. 3B), was 158.5 nm. Elemental EDX analysis performed on the red-marked area on the SEM image revealed the presence of 7.24 wt% nickel, 29.1 wt% carbon, 36.3 wt% oxygen, and nearly 1 wt% chlorine originating from $NiCl_2$ used during the Ni modification process.

3.1.5. Active surface area determination

The active surface area of Ni-CSNPs-SPCE, CSNPs-SPCE, and SPCE was determined via CV in 5 mM $K_3[Fe(CN)_6]/K_4[Fe(CN)_6]$ in 1 M KCl and calculated following the Randles–Ševčík equation (Eq. (5)):

$$I_p = 0.4463nFAC\left(\frac{nFvD}{RT}\right)^{1/2} \quad (5)$$

where I_p is the current maximum in A, n refers to the number of transferred electrons, A indicates the electrode area in cm^2, C is the concentration of the electroactive species in $molcm^{-3}$, v denotes the scan rate in Vs^{-1}, D is the diffusion coefficient in cm^2s^{-1}, R is the gas constant in $JKmol^{-1}$, F is the Faraday constant in C mol^{-1}, and T is the temperature in K. The calculated values of the active surface area of Ni-CSNPs-SPCE, and CSNPs-SPCE were compared with that of unmodified SPCE. The current responses of unmodified SPCE and CSNPs-SPCE were almost identical. An increase in current response was observed in the case of Ni-CSNPs-SPCE (Fig. 4). The calculated values of electroactive surface area

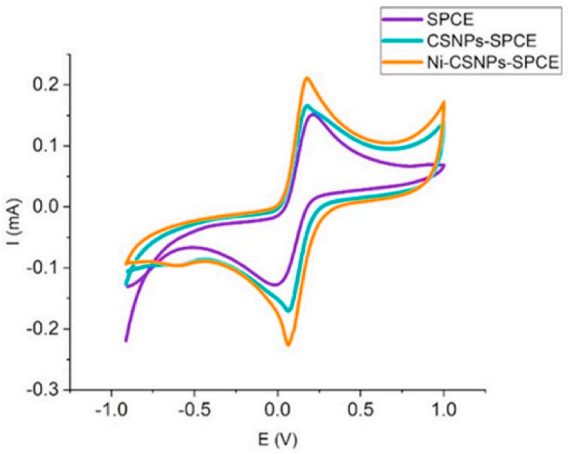

Fig. 4. Cyclic voltammograms of 5 mM $K_3[Fe(CN)_6]/K_4[Fe(CN)_6]$ in 1 M KCl at SPCE (violet line), CSNPs-SPCE (turtle line), and Ni-CSNPs-SPCE (orange line) with scan rate of 0.1 V/s. (For interpretation of the references to colour in this figure legend, the reader is referred to the Web version of this article.)

of unmodified SPCE, CSNPs-SPCE, and Ni-CSNPs-SPCE were as high as 0.18, 0.2, and 0.25 cm^2, respectively. The current response increase could be caused by larger nanoparticles size (Silah and Uslu, 2024). Based on the TEM result was Ni-CSNPs approx. 1.2-times bigger in comparison to CSNPs. Also, the active electrode surface area is 1.25-times larger in case of Ni-CSNPs in comparison to CSNPs. Based on the obtained results, Ni-CSNPs-SPCE exhibited the highest active surface area and provided the highest number of active sites on the electrode surface, leading to efficient analyte determination.

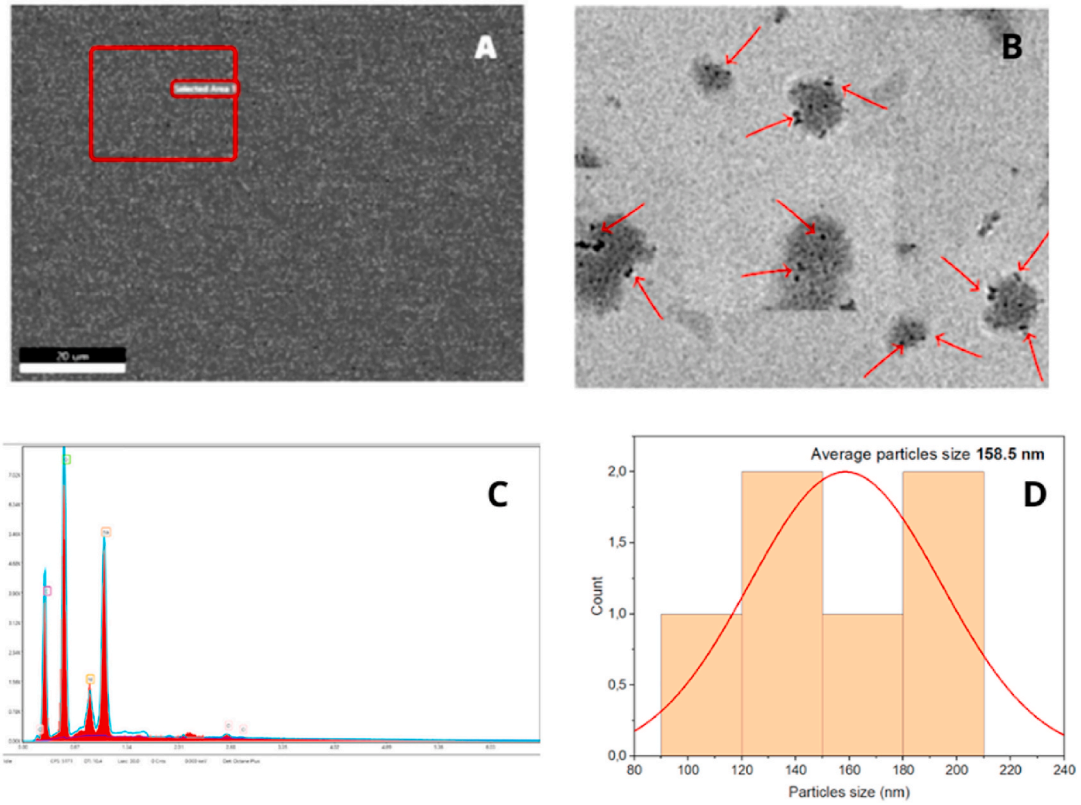

Fig. 3. SEM image of Ni-CSNPs at a scale of 20 μm (A). TEM image of Ni-CSNPs at scale of 0.5 μm; (B) and EDX spectrum of Ni-CSNPs (C) and histogram (D) of CSNPs size according to TEM image.

3.2. Impact of pH on electrochemical insulin determination on Ni-CSNPs-SPCE and the mechanism of insulin electrochemical oxidation

To study the impact of pH to electrochemical conditions for further insulin detection, insulin with a concentration of 2 μM was determined in three solutions with different pH values (2, 7.4, and 11) at Ni-CSNPs-SPCE. As shown in Fig. 5, different pH conditions strongly affect the shape of cyclic voltammograms and current response of the system. No obvious peaks were found for the determination of insulin in solution with acidic (Fig. 5 A, turtle line) and neutral pH (Fig. 5 A, violet line). Acidic pH can also affect the Ag reference electrode used. The higher current response corresponding to higher concentration of OH^- in solution (higher pH) indicates that the OH^- groups are engaged in the electrochemical reaction mechanism (Fig. 5 A, orange line). Proposed mechanism of insulin oxidation on the surface of Ni-CSNPs-SPCE in alkaline solution can be represented as follows (Equations (6) and (7))

$$\boldsymbol{Ni(OH)_2 + OH^- \rightarrow NiO(OH) + H_2O + e^-} \quad (6)$$

$$\boldsymbol{NiO(OH) + insulin \rightarrow Ni(OH)_2 + product} \quad (7)$$

$Ni(OH)_2$ particles are formed during the activation process of working electrodes. The NiO(OH) species formed during the electrochemical oxidation of insulin at alkaline pH in the presence of NaOH on Ni-CSNPs-SPCE represent the active sites, which strongly catalyze the direct oxidation of insulin (Equation (7)). The -OH groups of bioanalytes can interact with the -OH groups created during the electro-oxidation process (the process takes a place at the potential 0.8 V (Fig. 5 A, orange line),). So, there is the possibility to detect insulin, because the peak current is influenced by concentration of insulin. The modification of working electrode influence current response dramatically (Fig. 5 B). There were not obvious oxidation peak for SPCE or chitosan-SPCE electrodes. In the case of Ni-CSNPs-SPCE, there was one oxidation peaks at potential 0.8 V as was mentioned above. Two reduction peaks were observed around the potential 0.4 V. It could be expected that the reduction peaks pertain to the reduction of amino acids of insulin and reduction of NiO(OH) to $Ni(OH)_2$. Based on the results obtained insulin solutions containing 0.1 M NaOH with pH = 11 were used for all following electrochemical experiments.

3.2.1. Study of the kinetics of insulin oxidation on Ni-CSNPs-SPCE

To study the kinetic parameters of insulin oxidation in more details, CV curves of 2 μM insulin (pH = 11) insulin were recorded at different scan rates (25–200 mVs^{-1}). Fig. 6 shows the cyclic voltammograms of 2 μM insulin (pH = 11) on Ni-CSNPs-SPCE (Fig. 6A) at various scan rates with linear regression (Fig. 6A–D). Fig. 6 demonstrates the dependence of the maximum current value corresponding to the insulin oxidation (I) on the scan rate (v) on Ni-CSNPs-SPCE (Fig. 6B) as well as the dependence of I on square root of v (Fig. 6C) and log I on log v (Fig. 6D). All dependences were fitted with a linear function. In all cases, the dependences were linear with the $R^2 = 0.99$ (Fig. 6B–D). The linear dependence of log I on log v exhibited the following linear regression equation: $\log I = 1.07 \log v - 2.48$, which indicated the occurrence of an adsorption-controlled process based on equation 8

$$i_P = \frac{n^2F^2vA\Gamma}{4RT} = \frac{nFQv}{4RT} \quad (8)$$

where Q is the peak area. The results corresponds to the proposed mechanism above, the rate determining step is the adsorption of insulin on the top of working electrode, where are NiO(OH) active sites.

Based on the CV voltammograms the oxidation peak shifted positively (to higher potential values). A good linear relationship was observed between the oxidation potential (Ep) and ln v, as shown in Fig. 7. Based on the Laviron theory for irreversible process, it is possible to use the following equation:

$$E_P(V) = E^{0'} - \frac{RT}{\alpha nF} ln \frac{RTk_s}{\alpha nF} + \frac{RT}{\alpha nF} \ln v \quad (9)$$

Where $E^{0'}$ is the formal standard potential, k_s is the standard heterogenous reaction rate constant, and n, α, v, R, T, and F have usual meaning. Based on the mechanism of electrochemical reaction $n = 1$ and the $\alpha = 0.5$, which is typical for irreversible process. The formal standard potential was calculated from the linear relation of E_P vs. v (Fig. 7, inset). The value of this potential was 0.6 V. Then the heterogenous reaction rate constant was calculated according to equation (9) and its value was $5.39.10^{-3}$ s^{-1}. According to results, the electrode reaction is one electron electro-oxidation irreversible process.

3.2.2. Electrochemical determination of insulin on Ni-CSNPs-SPCE

3.2.2.1. Electrochemical determination of insulin on Ni-CSNPs-SPCE in simulated human body fluids. Based on the literature, it is known that the Ni-modified substrate can be used as a platform for insulin determination (Shepa et al., 2021; Hovancova et al., 2018; Silah and Uslu, 2024). Moreover, the properties of Ni-CSNPs, such as higher conductivity in comparison to the chitosan film and catalytic activity of NiO(OH) species, may lead to the development of an interesting platform for the determination of insulin. Therefore, various insulin concentrations (0.3 μM–5 μM) were determined using the developed Ni-CSNPs-SPCE by dropping 50 μL of insulin solution on the electrode surface. Fig. 8 shows

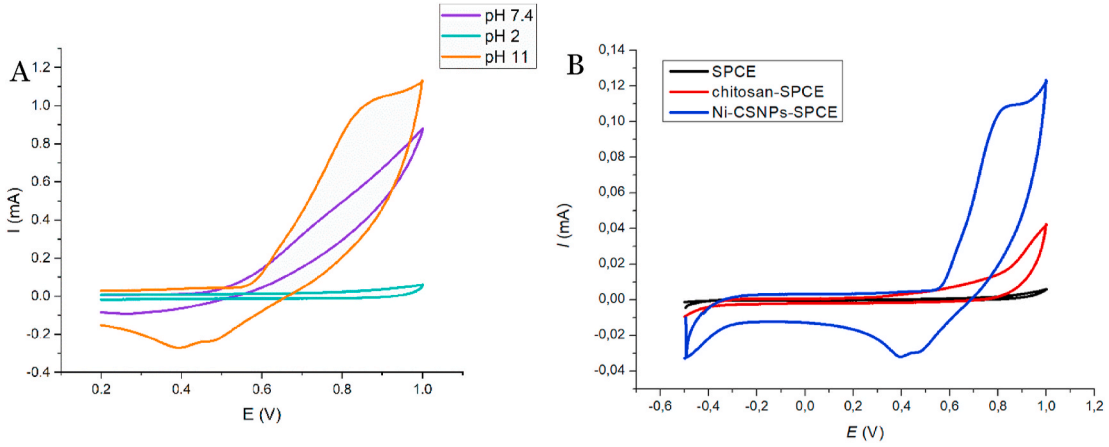

Fig. 5. Cyclic voltammograms of 2 μM insulin in PBS (violet line), in 0.1M HCl in PBS (turtle line), and in 0.1 M NaOH and PBS (orange line) at Ni-CSNPs-SPCE at scan rate of 0.1 Vs^{-1} (A). Cyclic voltammograms of 2 μM insulin in PBS (pH = 11) on SPCE (black line), chitosan-SPCE (red line), and Ni-CSNPS-SPCE (blue line) (B). (For interpretation of the references to colour in this figure legend, the reader is referred to the Web version of this article.)

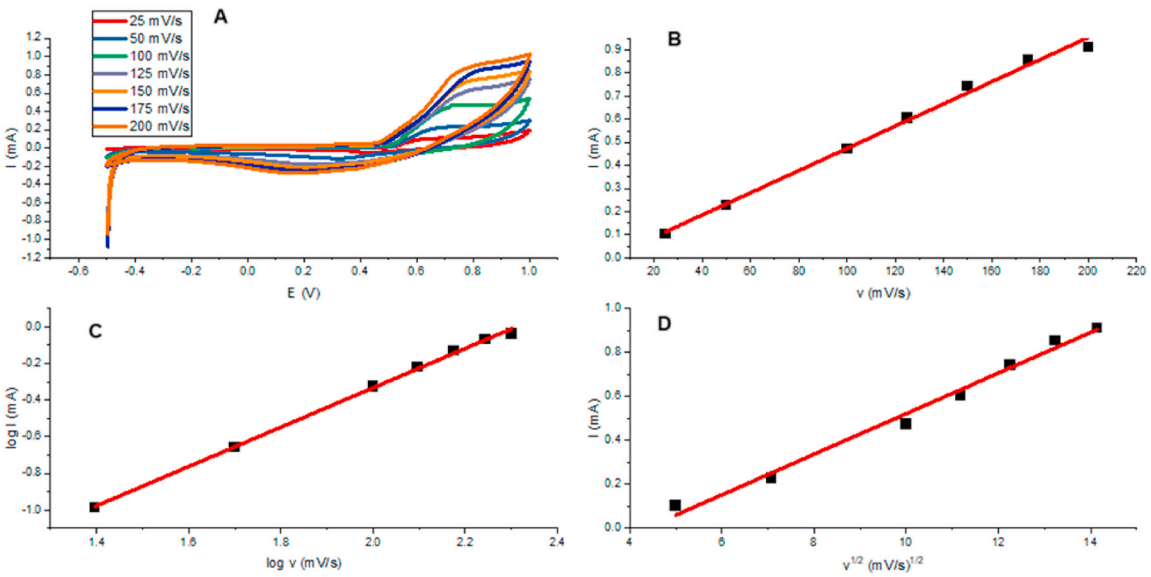

Fig. 6. Cyclic voltammograms of 2 μM insulin (pH = 11) on Ni-CSNPs-SPCE at different scan rates (A). The dependence of peak current on the scan rate (B), the dependence of peak current of log *I* on log *v* (C) and the dependence of peak current on the square root of scan rate (D).

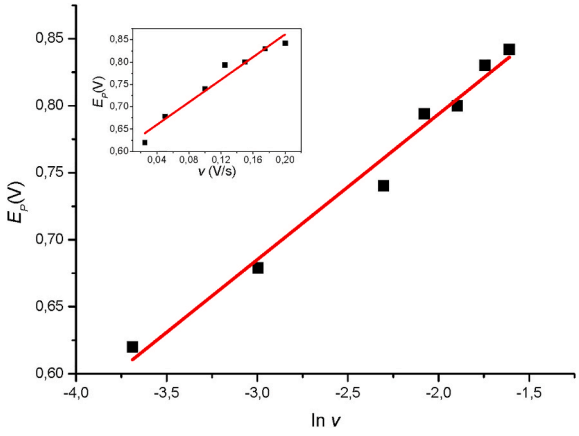

Fig. 7. The dependence of peak potential on the ln *v*. (Inset: The dependence of peak potential on scan rate).

the cyclic voltammograms of insulin solution with different concentrations (0.3 μM–5 μM) on Ni-CSNPs-SPCE in potential range from 0.2 V to 1 V at a scan rate of 0.1 V/s. The maximum current values corresponding to insulin oxidation process were observed at a potential of $E = +0.8$ V and increased linearly with increasing insulin concentration, as shown in Fig. 8. These results were fitted with a linear function $I = 0.088c + 0.067$ (Fig. 8B) and the correlation coefficient R^2 expressing the linearity of the given dependency ($R^2 = 0.99$) was observed and the sensing characteristics of the Ni-CSNPs-SPCE were calculated. Ni-CSNPs-SPCE exhibits a wide linear range (0.3 μM–5 μM), high sensitivity of 0.09 mA/μM and low limit of detection (LOD = 0.02 μM). The LOD was calculated from linear regression using the following equation (Equation (10)):

$$LOD = \frac{3.S_a}{b} \tag{10}$$

where S_a indicates the standard deviation of the response and b is the slope of the calibration curve. All measurements were performed 5 times, and the average value of current response was used to ensure the reproducibility of the developed sensor. The measurements were realized using 5 Ni-CSNPs-SPCEs modified in the same way. The calculated reproducibility was approx. 90 % for the concentration in the middle of linear range. The electroanalytical properties of the modified electrode were compared with other electrode modifications from the literature (Table 2). The modified electrode exhibits higher sensitivity in literature even when the linear range was wider than displays most of the previously reported modifications for insulin determination. For example, Ni-CSNPs-SPCE electrode shows a wider linear range for insulin

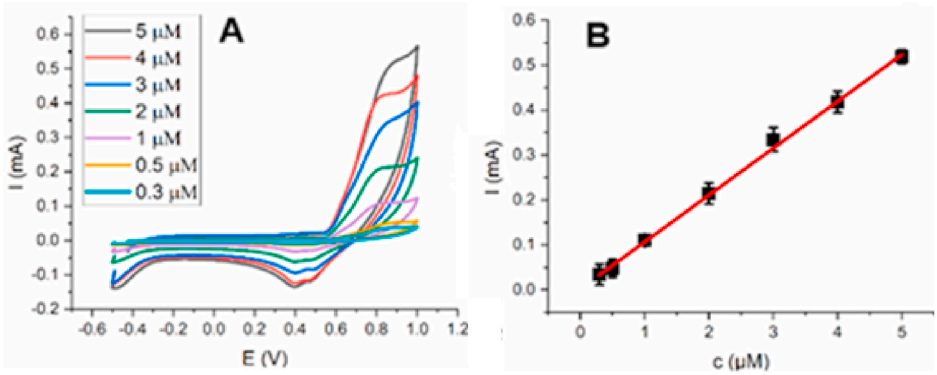

Fig. 8. Cyclic voltammograms of various insulin concentrations (0.3 μM–5 μM) in PBS and 0.1 M NaOH at scan rate of 0.1 V s-1 in a potential range −0.5 V to +1 V (A). The dependence of peak current on the insulin concentration fitted by a linear function (B).

Table 2
Analytical characteristics of various modified electrodes for insulin determination using electrochemical techniques.

Electrode	Method	Linear range	Limit of detection	Sensitivity	Literature
Ni-CSNPs-SPCE	CV	0.3 μM–5 μM	0.02 μM	0.09 mA μM^{-1}	This work
NiONPs/MWCNTs/SPCE	CV	1 μM–3 μM	4.51 μM	0.031 μA μM^{-1}	Pariente et al. (2015)
NiNPs/chitosan-MWCNTs/PGE	CV	1 μM–5 μM	4.34 μM	0.12 μA μM^{-1}	Hovancová et al. (2017)
NiNPs-PPy-SPCE	CV	0.5 μM–5 μM	90 nM	6.65 μA μM^{-1}	Šišoláková et al. (2023)
SPCE/NiONPs-Naftion-MWCNT	Amp.	20 nM–0.26 μM	6.1 nM	1.83 μA μM^{-1}	Rafiee and Fakhari (2013)
MWCNTs/dihydropyran composite film electrode	–	0.8 μM–2.5 μM	1 μM	1.33 nA μM^{-1}	Snider et al. (2008)
GCE/Chitosan/MWCNT	Amp.	0.1 μM–5 μM	30 nM	–	Zhang et al. (2005)
ZnNPs/chitosan-MWCNTs/SPCE	CV	0.5 μM–5 μM	0.28 μM	0.087 mA μM^{-1}	Šišoláková et al. (2021)
NiNPs/carbon fibre microelectrode	CV	2 μM–20 μM	270 nM	1.11 nA μM^{-1}	Lu et al. (2018)

determination than NiNPs-Ppy-SPCE or NiNPs-chitosan-MWCNTs-PGE. Insulin was determined via CV for all the mentioned electrodes. The electrode SPCE-NiO-Nafion-MWCNTs shows a wider linear range compared to prepared electrodes. However, insulin was determined by a different electrochemical method - amperometry. A comparison between prepared electrodes with ZnNPs-chitosan-MWCNTs-SPCE demonstrated the better analytical properties for Ni-CSNPs-SPCE.

3.2.2.2. Electrochemical determination of insulin on Ni-CSNPs-SPCE in presence of interferents. Selectivity of Ni-CSNPs-SPCE was studied using the cyclic voltammetry method in electrolyte containing the most common interferences (0.1 mM ascorbic acid, 0.1 mM saccharose, and 0.5 mM uric acid). Interference samples were prepared in phosphate-buffered saline (PBS) without insulin present in the solution.

The concentration of all biomolecules use was the same as their expected values in the blood samples. Moreover, all electrochemical measurements in this work were done in the PBS solution provided the same concentration of Cl^- ions as in human blood. As can be seen in Fig. 8 there was no oxidation peak observed at the potential corresponding to insulin oxidation on Ni-CSNPs-SPCE in the solutions containing the above-mentioned interferences. Fig. 9 also shows the CVs of 2 μM insulin (orange line). Based on these results further electrochemical determination of insulin in human blood was performed.

3.2.3. Electrochemical determination of insulin on Ni-CSNPs-SPCE in human blood

To assess the applicability to real samples, Ni-CSNPs-SPCE was used to determine insulin in human blood serum. The serum was used instead of PBS in CV measurements to study the current response of insulin with concentration of 5 μM, 2 μM, 1 μM, and 0.3 μM (Fig. 10A). The current response increased linearly with increasing insulin concentration in blood serum. These results were fitted with linear function (Fig. 10B) with correlation coefficient $R^2 = 0.99$ and the sensing properties of the Ni-CSNPs-SPCE in real samples were calculated according to Equation (5). The calculated LOD in human blood serum was 0.02 μM and the sensitivity was 0.12 mA/μM. According to these results, the prepared modified screen-printed electrode can be considered as a promising candidate for insulin detection in real samples.

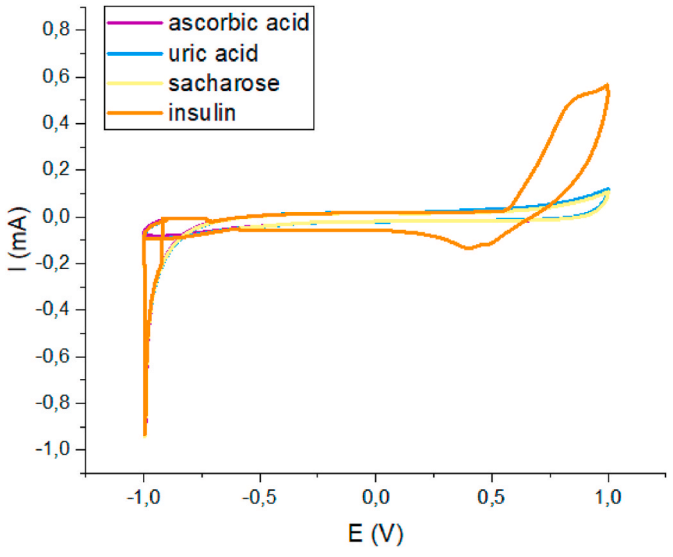

Fig. 9. Cyclic voltammograms of 2 μM insulin in PBS (orange line) Cyclic voltammograms for different interferences present in the blood (0.1 mM ascorbic acid, 0.5 mM uric acid, 0.1 mM sucrose) pH = 11. (For interpretation of the references to colour in this figure legend, the reader is referred to the Web version of this article.)

4. Conclusion

In summary, this study focused on the preparation of Ni-modified CSNPs for their potential application in electrochemical sensors for insulin detection. The spherical chitosan particles were successfully synthesized and display higher conductivity in comparison to chitosan films. Moreover, the FT-IR study results confirm the bond creation between the chitosan and TPP. Also, the complex creation between the chitosan NPS and Ni^{2+} ion. The Ni active sites in the structure were in situ transformed into the $Ni(OH)_2$ particles, which plays key role in the electrochemical oxidation of insulin. The electrochemical measurements display that the oxidation reaction of the insulin is the irreversible one electron reaction limited by adsorption of insulin on electroactive species NiO(OH). Based on these theoretical knowledges, the electroanalytical parameters for insulin determination on modified electrode were calculated. The insulin was determined within a wide linear range from 300 nM to 5 μM with sensitivity 0.09 mA/μM and detection limit 20 nM. The achieved results are better than electroanalytical properties of sensors with common modification found in literature. The studied sensor was able to determine insulin not only in the presence of selected interference, but also in blood serum. Proposed results determined the studies sensor Ni-CSNPs-SPCE as promising platform for future application in insulin real samples determination.

Ethical approval

Not applicable.

CRediT authorship contribution statement

Frederika Chovancová: Data curation. **Marjan Motiei:** Writing – original draft, Methodology, Data curation. **Ivana Šišoláková:** Writing – review & editing, Writing – original draft, Supervision, Methodology, Funding acquisition, Data curation, Conceptualization. **Michal Urbánek:** Writing – original draft, Data curation. **Jana Shepa:** Writing – review & editing, Supervision. **Haojie Fei:** Data curation. **Petr Sáha:** Supervision. **Renáta Oriňaková:** Writing – review & editing, Supervision.

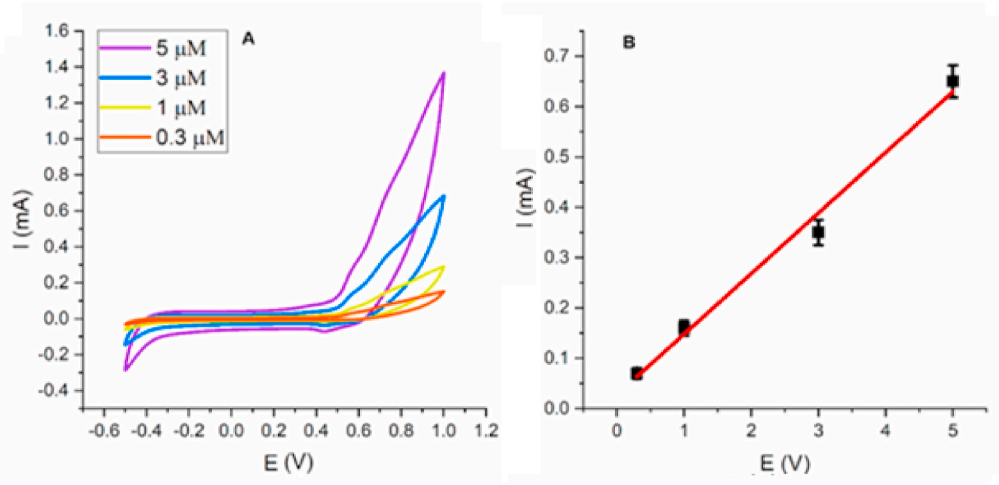

Fig. 10. Cyclic voltammograms of different insulin concentrations on Ni-CSNPs-SPCE at a scan rate of 50 mV/s (A) in blood serum with 0.1 M NaOH. The dependence of peak current on the insulin concentration, as fitted by a linear function (B).

Availability of data and materials

Data available on request from the authors. The data that support the findings of this study are available from the corresponding author (IŠ) upon reasonable request.

Declaration of competing interest

The authors declare that they have no known competing financial interests or personal relationships that could have appeared to influence the work reported in this paper.

Acknowledgements

This research work has been supported by the project NATO SPS program ID number G6106, and by the EU NextGenerationEU through the Recovery and Resilience Plan for Slovakia under the project No. 09I03-03-V04-00180.

Data availability

Data will be made available on request.

References

Algharib, S.A., et al., 2022. Preparation of chitosan nanoparticles by ionotropic gelation technique: effects of formulation parameters and in vitro characterization. J. Mol. Struct. 1252 (Mar). https://doi.org/10.1016/j.molstruc.2021.132129.

Bhattacharjee, S., 2016. DLS and zeta potential - what they are and what they are not? J. Contr. Release 235, 337–351. https://doi.org/10.1016/j.jconrel.2016.06.017.

Ciszewski, A., Stepniak, I., 2013. Deposition of nickel hydroxide nanoparticles derivatized from nickel chitosan complex on glassy carbon electrode for oxidative electrocatalysis. Int. J. Electrochem. Sci. 8 (5), 6377–6392. https://doi.org/10.1016/s1452-3981(23)14769-9.

Cruz-Pineda, W.D., Parra-Rojas, I., Rodríguez-Ruíz, H.A., Illades-Aguiar, B., Matia-García, I., Garibay-Cerdenares, O.L., 2022. The regulatory role of insulin in energy metabolism and leukocyte functions. J. Leukoc. Biol. 111 (1), 197–208. https://doi.org/10.1002/JLB.2RU1220-847R.

Dong, X., et al., 2020. Ultrasensitive detection of chloramphenicol using electrochemical aptamer sensor: a mini review. Electrochem. Commun. 120, 106835. https://doi.org/10.1016/j.elecom.2020.106835.

El-Naggar, N.E.A., El-Shall, H., Elyamny, S., Hamouda, R.A., Eltarahony, M., 2024. Novel algae-mediated biosynthesis approach of chitosan nanoparticles using Ulva fasciata extract, process optimization, characterization and their flocculation performance. Int. J. Biol. Macromol. 282 (P3), 136925. https://doi.org/10.1016/j.ijbiomac.2024.136925.

Hovancová, J., Šišoláková, I., Oriňaková, R., Oriňak, A., 2017. Nanomaterial-based electrochemical sensors for detection of glucose and insulin. J. Solid State Electrochem. 21 (8), 2147–2166. https://doi.org/10.1007/s10008-017-3544-0.

Hovancova, J., Orin, A., Garcia, D.R., Shylenko, O., Radon, J., 2018. Comparison of Insulin Determination on NiNPs/Chitosan-MWCNTs and NiONPs/Chitosan-MWCNTs Modified Pencil Graphite Electrode, pp. 1–11. https://doi.org/10.1002/elan.201800483.

Ibáñez-Redín, G., Wilson, D., Gonçalves, D., Oliveira, O.N., 2018. Low-cost screen-printed electrodes based on electrochemically reduced graphene oxide-carbon black nanocomposites for dopamine, epinephrine and paracetamol detection. J. Colloid Interface Sci. 515, 101–108. https://doi.org/10.1016/j.jcis.2017.12.085.

Islam, S., Bhuiyan, M.A.R., Islam, M.N., 2017. Chitin and chitosan: structure, properties and applications in biomedical engineering. J. Polym. Environ. 25 (3), 854–866. https://doi.org/10.1007/s10924-016-0865-5.

Ivanov, R., Czibula, C., Teichert, C., Bojinov, M., Tsakova, V., 2021. Carbon screen-printed electrodes for substrate-assisted electroless deposition of palladium. J. Electroanal. Chem. 897 (March), 115617. https://doi.org/10.1016/j.jelechem.2021.115617.

Khoerunnisa, F., et al., 2021. Physicochemical properties of TPP-Crosslinked chitosan nanoparticles as potential antibacterial agents. Fibers Polym. 22 (11), 2954–2964. https://doi.org/10.1007/s12221-021-0397-z.

Kuyukina, M.S., V Makarova, M., Pistsova, O.N., Glebov, G.G., Osipenko, M.A., Ivshina, I. B., 2022. Heliyon Exposure to metal nanoparticles changes zeta potentials of Rhodococcus cells. Heliyon 8 (April), e11632. https://doi.org/10.1016/j.heliyon.2022.e11632.

Le, N.T., Myrick, J.M., Seigle, T., Huynh, P.T., Krishnan, S., 2018. Mapping electrospray modes and droplet size distributions for chitosan solutions in unentangled and entangled concentration regimes. Adv. Powder Technol. 29 (12), 3007–3021. https://doi.org/10.1016/j.apt.2018.10.006.

Lu, L., Liang, L., Xie, Y., Tang, K., Wan, Z., Chen, S., 2018. A nickel nanoparticle/carbon nanotube-modified carbon fiber microelectrode for sensitive insulin detection. J. Solid State Electrochem. 22 (3), 825–833. https://doi.org/10.1007/s10008-017-3816-8.

Mao, A., Li, H., Yu, L., Hu, X., 2017. Electrochemical sensor based on multi-walled carbon nanotubes and chitosan-nickel complex for sensitive determination of metronidazole. J. Electroanal. Chem. 799 (April), 257–262. https://doi.org/10.1016/j.jelechem.2017.05.049.

Motiei, M., Kashanian, S., Lucia, L.A., Khazaei, M., 2017. Intrinsic parameters for the synthesis and tuned properties of amphiphilic chitosan drug delivery nanocarriers. J. Contr. Release 260 (June), 213–225. https://doi.org/10.1016/j.jconrel.2017.06.010.

Motiei, M., Sedlařík, V., Lucia, L.A., Fei, H., Münster, L., 2020. Stabilization of chitosan-based polyelectrolyte nanoparticle cargo delivery biomaterials by a multiple ionic cross-linking strategy. Carbohydr. Polym. 231 (June 2019). https://doi.org/10.1016/j.carbpol.2019.115709.

Musa, A.M., Kiely, J., Luxton, R., Honeychurch, K.C., 2021. Recent progress in screen-printed electrochemical sensors and biosensors for the detection of estrogens. TrAC, Trends Anal. Chem. 139, 116254. https://doi.org/10.1016/j.trac.2021.116254.

Naskar, A., Guha, A.K., Mukherjee, M., Ray, L., 2016. Adsorption of nickel onto Bacillus cereus M116: a mechanistic approach. Separ. Sci. Technol. 51 (3), 427–438. https://doi.org/10.1080/01496395.2015.1115069.

Netskina, O.V., Pochtar, A.A., Komova, O.V., Simagina, V.I., 2020. Solid-state naBH4 composites as hydrogen generation material: Effect of thermal treatment of a catalyst precursor on the hydrogen generation rate. Catalysts 10 (2). https://doi.org/10.3390/catal10020201.

Othman, S.I., Alturki, A.M., Abu-Taweel, G.M., Altoom, N.G., Allam, A.A., Abdelmonem, R., 2021. Chitosan for biomedical applications, promising antidiabetic drug delivery system, and new diabetes mellitus treatment based on stem cell. Int. J. Biol. Macromol. 190 (August), 417–432. https://doi.org/10.1016/j.ijbiomac.2021.08.154.

Parasuraman, S., Rao, A., Balamurugan, S., Muralidharan, S., Jayaraj Kumar, K., Vijayan, V., 2015. An overview of liquid chromatography-mass spectroscopy instrumentation. Pharmaceutical Methods 5 (2), 47–55. https://doi.org/10.5530/phm.2014.2.2.

Pariente, F., et al., 2015. Insulin sensor based on nanoparticle-decorated multiwalled carbon nanotubes modified electrodes. Sensors and Actuators B: Chemical 222, 331–338. https://doi.org/10.1016/j.snb.2015.08.033.

Przybylska, A., Gackowski, M., Koba, M., 2021. Application of capillary electrophoresis to the analysis of bioactive compounds in herbal raw materials. Molecules 26 (8), 1–24. https://doi.org/10.3390/molecules26082135.

Rafiee, B., Fakhari, A.R., 2013. Author ' s accepted manuscript. Biosensors and Bioelectronic. https://doi.org/10.1016/j.bios.2013.01.037.

Ribeiro, M.C., et al., 2018. Improving peptide quantification in chitosan nanoparticles. Int. J. Biol. Macromol. 119, 32–36. https://doi.org/10.1016/j.ijbiomac.2018.07.119.

Seyam, S., Choukaife, H., Al Rahal, O., Alfatama, M., 2024. Colonic targeting insulin-loaded trimethyl chitosan nanoparticles coated pectin for oral delivery: in vitro and in vivo studies. Int. J. Biol. Macromol. 281 (P4), 136549. https://doi.org/10.1016/j.ijbiomac.2024.136549.

Shepa, J., et al., 2021. Nio nanoparticles for electrochemical insulin detection. Sensors 21 (15), 12–17. https://doi.org/10.3390/s21155063.

Silah, H., Uslu, B., 2024. Journal Pre-proof Nanotechnology based electrochemical (bio) sensors for insulin/hormone sensing. Curr. Pharm. Anal. https://doi.org/10.1016/j.cpan.2024.12.003.

Simos, Y.V., et al., 2021. Trends of nanotechnology in type 2 diabetes mellitus treatment. Asian J. Pharm. Sci. 16 (1), 62–76. https://doi.org/10.1016/j.ajps.2020.05.001.

Šišoláková, I., et al., 2020. Electrochemical determination of insulin at CuNPs/chitosan-MWCNTs and CoNPs/chitosan-MWCNTs modified screen printed carbon electrodes. J. Electroanal. Chem. 860. https://doi.org/10.1016/j.jelechem.2020.113881.

Šišoláková, I., et al., 2021. Zn nanoparticles modified screen printed carbon electrode as a promising sensor for insulin determination. Electroanalysis 33 (3), 627–634. https://doi.org/10.1002/elan.202060417.

Šišoláková, I., et al., 2023. Polymer-based electrochemical sensor: fast, accurate, and simple insulin diagnostics tool. Electrocatalysis, 0123456789. https://doi.org/10.1007/s12678-023-00827-w.

Snider, R.M., Ciobanu, M., Rue, A.E., Cliffel, D.E., 2008. A multiwalled carbon nanotube/dihydropyran composite film electrode for insulin detection in a microphysiometer chamber. Anal. Chim. Acta 609 (1), 44–52. https://doi.org/10.1016/j.aca.2007.12.032.

Vicente, W.C., Carli, L.N., Brondani, P.B., 2025. Recent advances in the application of chitosan nanoparticles for the modification of textiles. Prog. Org. Coating 198, 108910. https://doi.org/10.1016/j.porgcoat.2024.108910.

Vroman, I., Tighzert, L., 2009. Biodegradable polymers. Materials 2 (2), 307–344. https://doi.org/10.3390/ma2020307.

Yanat, M., Schroën, K., 2021. Preparation methods and applications of chitosan nanoparticles; with an outlook toward reinforcement of biodegradable packaging. React. Funct. Polym. 161 (December 2020), 104849. https://doi.org/10.1016/j.reactfunctpolym.2021.104849.

Yu, Y., Guo, M., Yuan, M., Liu, W., Hu, J., 2016. Nickel nanoparticle-modified electrode for ultra-sensitive electrochemical detection of insulin. Biosens. Bioelectron. 77, 215–219. https://doi.org/10.1016/j.bios.2015.09.036.

Zhang, M., Mullens, C., Gorski, W., 2005. Insulin oxidation and determination at carbon electrodes. Anal. Chem. 77 (19), 6396–6401. https://doi.org/10.1021/ac0508752.